PVDF/PLA electrospun fiber membrane impregnated with metal nanoparticles for emulsion separation, surface antimicrobial, and antifouling activities

XIANG Xin, CHEN DongYun*, LI NaJun, XU QingFeng, LI Hua, HE JingHui & LU JianMei*

College of Chemistry, Chemical Engineering and Materials Science, Soochow University, Suzhou 215123, China

Although many superwetting materials have been designed for the treatment of oil-containing wastewater, separation strategies for oil-in-water systems containing bacteria have rarely been reported. Herein, poly(vinylidene difluoride)- and poly(lactic acid)-blended fibrous membranes loaded with silver and copper oxide nanoparticles were successfully prepared by a two-step method of electrostatic spinning and liquid-phase synthesis. The product membrane showed excellent super-oleophilic properties in air and hydrophobicity under oil. It could separate water-in-oil emulsion systems containing surfactants with an efficiency above 90%. More importantly, the nanoparticle-loaded fibers were characterized by material degradability and slowly released ions. The fibers exhibited excellent antibacterial activities against both gram-positive and -negative bacteria. This work provides a feasible strategy for water-in-oil emulsion separation and bacterial treatment of wastewater.

emulsion separation, antibacterial activity, electrostatic spinning, Ag nanoparticles

1 Introduction

The rapid development of modern industry and population growth has intensified the discharge of industrial and domestic wastewater. Frequent offshore oil spills are cause for widespread concern regarding oil-contaminated waters [1,2]. Oily wastewater mainly comprises petroleum and organic solvents from various industries, such as pharmaceuticals, metallurgy, food processing, and petrochemicals. According to its composition and physical form, oily wastewater can be classified as an oil-water mixture, a free dispersion of oil-water emulsion, or a stable emulsion system containing an emulsifier. Of these, emulsions that contain surfactants with a particle size below 20 μm are the most difficult to separate [3,4]. In addition to their complex composition, such was-tewaters usually contain bacteria, dyes, heavy metal ions, and other hazardous substances. Traditional separation methods include those based on chemical, physical, biological, adsorption, flocculation, centrifugation, and electrochemical principles. However, these methods often cause secondary pollution, have high energy consumption, low efficiency of separation, or have other disadvantages [5]. Arising from the rapid advances in interface science and bionics, special wettability materials are considered promising candidates for oil-water separations because of their high separation efficiency and fast rate of separation. Membrane separation is an environmentally friendly, economical, and recyclable technology, which is widely used in water purification, seawater desalination, and liquid separation [6–8]. The design and preparation of intelligent, multifunctional, and shape-controlled liquid separation membranes for complex oil-water systems is a topic of significant

current research.

Water is the source of life. Contaminated water may contain pathogenic microorganisms. Trace amounts of nutrients in water provide an ideal place for bacteria to multiply. Direct contact or inadvertent oral ingestion can lead to infectious diseases. Therefore, pathogenic bacteria in drinking water are one of the biggest threats to public health [9,10]. In addition, growth and reproduction of microorganisms, such as iron and saprophytic bacteria, in oilfield water-injection systems often cause corrosion and blockage to extraction equipment and pipelines, which indirectly causes economic losses and environmental hazards [11,12]. Therefore, oily wastewater carrying microorganisms requires special treatment. The separation of emulsions containing surfactants is more challenging than that of oil-water mixtures. The membrane requirements are more stringent, not only in terms of size characteristics but require the membrane to have a reasonable pore structure [13–15]. The pore size should be smaller than the size of the emulsified oil droplets to provide interception, but not too small to affect the permeate flux and extrinsic driving pressure. Furthermore, the ideal membrane should have selective superwetting performance, which provides the intrinsic driving force for oil-water separation. The membrane also requires flexible physical and mechanical properties and reusability.

Nanofiber membranes prepared by electro-spinning exhibit controlled wettability, diverse fiber structures, excellent dispersion, and high specific surface area and porosity, and hence show great promise in treating emulsified oil-containing wastewater [16–20]. In addition, when such membranes are applied to antimicrobial applications, numerous studies have shown that the high specific surface area and porosity allow the antimicrobial agent to fully interact with external media [21–25]. For example, Wu et al. prepared a visible light-driven biocidal fibrous membrane by co-assembly [26]. Karagoz et al. [27] designed a fibrous membrane modified with zinc oxide nanorods and silver nanoparticles for protective clothing applications. Liu et al. [28] designed an electrospun membrane composed of chitosan, polylactic acid, and gelatine for food packaging and preservation. Pakravan et al. [29] prepared a core-shell structured electrospun fiber membrane for drug-retarding action with polyethylene oxide and chitosan.

Although electrostatic-spun fiber has a wide range of applications, considerably more research is required to achieve industrialization. One aspect that remains unclear is the reaction mechanism and special morphology [30–34].

Precious metals, such as silver and copper, have long been used in experimental studies as antibacterial agents. Trace amounts of silver ions can kill hundreds of bacteria, which far exceeds the antibiotic effect. Copper oxide particles are also used. Although their bactericidal effect is not as good as

that of silver, CuO is widely used in sterilization because of its simple preparation, low cost, and chemical stability. Silver and copper kill bacteria by similar mechanisms: when exposed to water, the metal becomes a cation that interacts with the surface of negatively charged bacteria, leading to cell rupture and microbial death. The reason for choosing two types of metal particles as additives in this work is that silver is better than copper oxide for sterilization, but is difficult to prepare and expensive. Owing to the degradability of poly(lactic acid) (PLA), the addition of copper oxide nanoparticles can greatly increase the surface area of the fiber, which makes it more conducive to contact of metal particles with a microbial surface and improves the antibacterial effect. In addition, it has been reported that certain amounts of silver and copper oxide used together can achieve an ideal bactericidal effect.

In this work, a hydrophobic and lipophilic film loaded with metal nanoparticles was prepared by a two-step method of electrostatic spinning and liquid-phase synthesis. The membrane successfully combined water purification and surface antibacterial activity functions. Scheme 1 shows the process of membrane preparation and emulsion separation. Copper oxide and silver nanoparticles were synthesized in water and polyol, respectively, and then blended into a degradable PLA spinning solution. The fiber was blended with poly(vinylidene difluoride) (PVDF) to improve its mechanical strength. PVDF also has low surface energy. The produced fiber membranes exhibited super-hydrophobicity and oleophilic properties, and were capable of separating water-in-oil emulsions. In addition, they showed excellent antibacterial properties against common microorganisms found in water, such as *Escherichia coli* (*E. coli*), *Pseudomonas aeruginosa* (*P. aeruginosa*), and *Bacillus subtilis*. This study provides a new concept for oil-water separation and surface antibacterial activity.
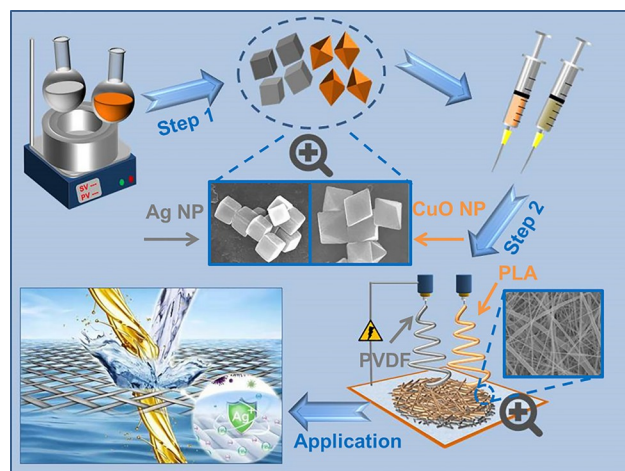
Scheme 1　(Color online) Illustration of membrane fabrication and emulsion separation.

2   Experimental procedures

2.1   Materials

Copper chloride dihydrate ($CuCl_2 \cdot 2H_2O$) and silver nitrate ($AgNO_3$, ≥99.8%) were purchased from Aladdin Co. (China). PVDF (MW400000) was obtained from Macklin Biochemical Co., Ltd. (China). PLA (MW100000) and polyvinylpyrrolidone (PVP; MW 30 000) were acquired from Sigma-Aldrich. The organic solvents: *N,N*-Dimethylformamide (DMF), *N,N*-Dimethylacetamide (DMAC), *n*-hexane, cyclohexane, isooctane, chloroform, methylene chloride, toluene, chlorobenzene, phenixin, and bromoethane, sodium dodecyl sulfate (SDS), cetyltriethylammonium bromide (CTAB), and Span-80 were purchased from Sinopharm Chemical Reagent Co. (China), as were phosphate-buffered saline (PBS), nutritional broth, and nutrient agar medium. Sodium hydroxide and ascorbic acid were procured from Maclean Biochemical Technology Co., Ltd. *Pseudomonas putida* (*P. putica*; ATCC 49128), *E. coli* (ATCC 25922), (*S. aureus* ATCC 29213), and *Bacillus subtilis* (ATCC 6633) were provided from Guangdong Institute of Microbiology (China). All chemical reagents were analytically pure: no further purification was required.

2.2   Fabrication of Ag nanoparticles

The synthesis of silver nanoparticles was improved from a previous method [35–41]. In a typical reaction, 25 mL of ethylene glycol was poured into a 100 mL flask and preheated to 150°C using an oil bath. The following solutions were prepared in advance: 1 mL of HCl (5 mmol L^{-1}) in ethylene glycol (EG), 3 mL of $AgNO_3$ (95 mmol L^{-1}) in EG, and 3 mL of PVP (150 mmol L^{-1}) in EG. Apart from the reagent addition, the entire process was conducted in a light-proof closed environment. HCl was pipetted into the flask, heated, and stirred for 15 min. The silver nitrate and PVP solutions were then slowly added to the flask by a dual-line titration method. On maintaining the temperature and stirring, the color of the reaction solution changed from milky white to clarified yellow to red. The final product was washed several times with acetone and deionized water.

2.3   Fabrication of CuO nanoparticles

The copper oxide nanoparticles were synthesized according to the method used in a previous study [42]. Morphological control was mainly achieved by adjusting the mass ratio of the dispersant PVP and the copper source. 0.171 g of $CuCl_2 \cdot 2H_2O$ was dissolved in 100 mL of deionized water and 3.33 g PVP was added the dispersant. The mixed solution was heated to 55°C and stirred for 15 min, then 10 mL of 2 mol L^{-1} sodium hydroxide solution was added to the flask and stirred for 30 min. Finally, 10 mL of the ascorbic acid

solution was added and the mixture was stirred for 1 h. The product was washed several times with ethanol and deionized water. The color of the solution changed from blue to green, and then to red during the process.

2.4   Electrospinning of PVDF/PLA@Ag/CuO nanofibers

PVDF powder (0.7 g) was weighed and dissolved in 1.7 g DMAC and 2.5 g acetone mixture and stirred for 12 h to a homogeneous solution. Copper oxide powder (0.1 g) was then added to the mixture and sonicated for 30 min. The PLA spinning solution comprised chloroform, methylene chloride, and DMF in a ratio of 1:1:1 by volume. The mass of PLA powder was 10% of the solution. Silver nanoparticles (0.1 g) were then added to the solution and sonicated for 30 min to complete dispersion. The parameters of the spinning machine were as follows: the positive and negative voltages were set to 20 kV and −5 kV, respectively; the acceptance distance was 15 cm, and the propulsion speed was 0.15 mm min^{-1}.

2.5   Preparation of water-in-oil emulsions

Several types of water-in-oil emulsions were produced via the following steps: 50 mg of emulsifier (Span-80, SDS, CTAB) was added to 100 mL of toluene, stirred thoroughly, and then 1 mL of deionized water was added. The mixed solution was stirred for several hours until the emulsion formed a homogeneous phase.

2.6   Emulsion separation experiment and cycle test

The fiber membrane was cut into squares of 4 cm in size, wetted with an organic solvent, and then attached to a filter device. Water-in-oil emulsion (20 mL) was slowly poured into the device, driven by 0.1 MPa pressure. The membrane was washed with ethanol and deionized water. The operation was repeated to test the recycling performance of the membrane.

The separation efficiency (R) was calculated by the following equation:

$$R = \left(1 - \frac{c}{c_0}\right) \times 100\%, \tag{1}$$

where C is the water concentration in the filtrate and C_0 is that in the original emulsion. The flux F (L m^{-2} h^{-1}) was calculated by the following equation:

$$F = \frac{V}{A \times t}, \tag{2}$$

where V (L) is the volume of emulsion passed, A (m^2) is the filtration area of the membrane, and t (h) is the filtration time.

2.7 Bacterial cultures

Bacillus subtilis, *E. coli*, and *P. aeruginosa* were employed to represent both gram-positive and -negative bacteria. All instruments were autoclaved and operational steps were performed under aseptic conditions. After the thawing of a strain, it was inoculated in 50 mL Luria-Bertani broth medium, then transferred to a water-bath shaker where it was held at 37°C for 24 h. The bacterial suspension was washed several times by centrifugation with phosphate-buffered saline (PBS). The bacteria were dispersed in the nutrient solution for subsequent experiments.

2.8 Evaluation of antibacterial performance of nanofiber membrane

The paper diffusion method was used to evaluate antibacterial performance. The fibrous membrane was cut into 1 cm radius discs using a hole punch. The treated bacterial suspension (1 mL) was added to the agar medium. The bacterial solution was uniformly painted onto the surface of the culture medium three times using a sterile cotton swab to ensure uniform application. The discs were then attached to the center and incubated in a thermostat at 37°C for 12 h to observe the size of the inhibition circle.

2.9 Characterization

The appearance of the membrane and morphologies of nanoparticles and microorganisms were observed by scanning electron microscopy (SEM; S-4700, Japan). Crystal structures of the nanoparticles were examined by X-ray diffraction (XRD; D8 QUEST, Germany). Elemental distributions and contents of the membranes were analysed by X-ray energy-dispersive spectroscopy (EDS). Possible forms of the chemical elements were determined using X-ray photoelectron spectroscopy (XPS; ESCALAB 250Xi, Germany).

Changes in the membrane before and after lamination were compared by Fourier transform infrared spectroscopy (FTIR; Nicolet 4700, USA). The wettability of the membrane was measured with an optical contact angle meter (OCA; 15EC, Germany). The morphology of the water-in-oil droplets was observed by light microscopy (Leice; BM2000, Germany). The droplet size distributions before and after separation were measured by dynamic light scattering (DLS; ZEN3690, UK). The surface area and porosity of the membrane were measured by Brunauer-Emmett-Teller gas absorptometry (BET; ASAP2460, USA). The antibacterial activity of the membranes was indicated by the inhibition circles formed on agar plates.

3 Results and discussion

3.1 Morphology and structure

The morphology of the metal particles was observed by electron microscopy (Figure 1(a)–(f)). The CuO nanoparticles were ortho-octahedral with a size of approximately 500 nm; the Ag nanoparticles were octahedra with a size of 200–300 nm. A comparison of images taken before and after spinning showed that the nanoparticles were uniformly embedded in the nanofibers. The diameter of PVDF fibers is about 100 nm, which is slightly larger than the diameter of PLA. This led to an increase in the specific surface area of the membrane and a slight decrease in the pore size (Figure S1), which resulted in better emulsion-breaking.

3.2 Elemental distribution and structural characterization

Figure 2 shows XRD patterns of the metal nanoparticles [35]. The positions of the CuO diffraction peaks proved its successful synthesis. The evolution of the Ag nanoparticles was indicated by changes in the positions of the diffraction
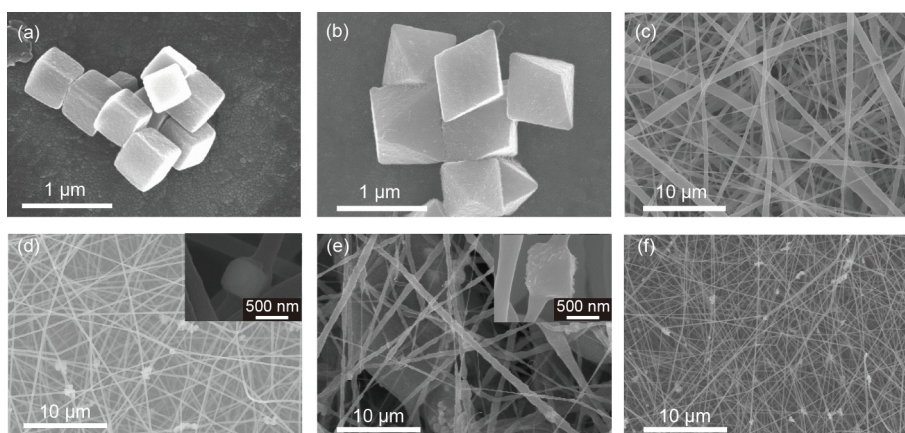

Figure 1 Scanning electron microscopy images of (a) Ag nanoparticles, (b) CuO nanoparticles, (c) PVDF/PLA electrospun nanofiber membrane, (d) PLA nanofibers with Ag nanoparticles, (e) PVDF nanofibers with CuO nanoparticles, (f) PVDF/PLA electrospun fiber membrane with metal nanoparticles.
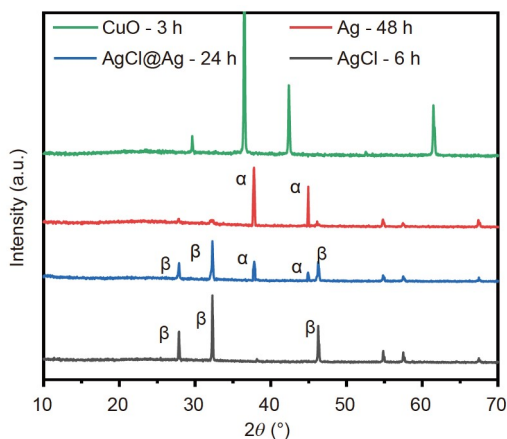
Figure 2 (Color online) X-ray diffraction patterns of CuO and Ag nanoparticles.

peaks, where the α-peaks are attributed to Ag and the β-peaks to AgCl. The corresponding SEM images are shown in Figure S2. When no chloride ions were involved, the silver crystals grew as aggregates, mostly in the form of lines, and the solution was milky white; when chloride ions were involved, the morphology appeared as random particles of micron size and with a relatively rough surface. As the reaction continued, the color of the solution changed from clarified yellow to turbid red, and the particles were in the form of regular nano cubes. Figure S3 shows ultraviolet-visible absorption spectra of the aqueous solutions that contained silver nano cubes [37].

XPS analysis of the product films was performed. Analyses of the carbon, oxygen, fluorine, copper, and silver peaks are shown in Figure 3(a)–(f). The Cu 2p (~952 and ~931 eV) and Ag 3d (~373 and ~366 eV) peaks proved

successful synthesis of the composite membrane as well as the presence of C=O and C–O. An EDS scan (Figure 4) also detected the presence of all elements. FTIR spectra of the individual and composite PVDF and PLA fiber membranes were measured (Figure 5) [43]. The distribution of functional groups further proved the successful synthesis of the target materials.

3.3 Wettability of membrane surface

The surface wettability of the composite membrane was characterized by measuring the surface contact angle. As shown in Figure 6, the membranes exhibited superhydrophobic and super-oleophilic properties in air, but oleophilic properties under water and superhydrophobic properties under oil. This allowed the formation of a hydrophobic oil layer on the surface when the oil passed through the membrane, which was theoretically capable of separating water-in-oil emulsions. The theoretical model is shown in Figure 7(a). Crucial to the separation are the breakthrough pressure (ΔP) and pore size. According to Young's equation, the pressure of a liquid penetrating into the pore surface is given by

$$\Delta P = \frac{-2\gamma\cos\theta}{r},\qquad(3)$$

where γ represents the liquid surface tension, θ is the liquid surface contact angle, and r is the pore radius. When θ is less than 90°, ΔP is less than zero, and surface oil droplets can wet the surface and spontaneously penetrate through the membrane. Owing to the hydrophobicity under oil, θ is greater than 90°, so water droplets are blocked from passing through the upper layer.

To demonstrate its universality, the contact angles of other organic reagents under liquid were also measured. The
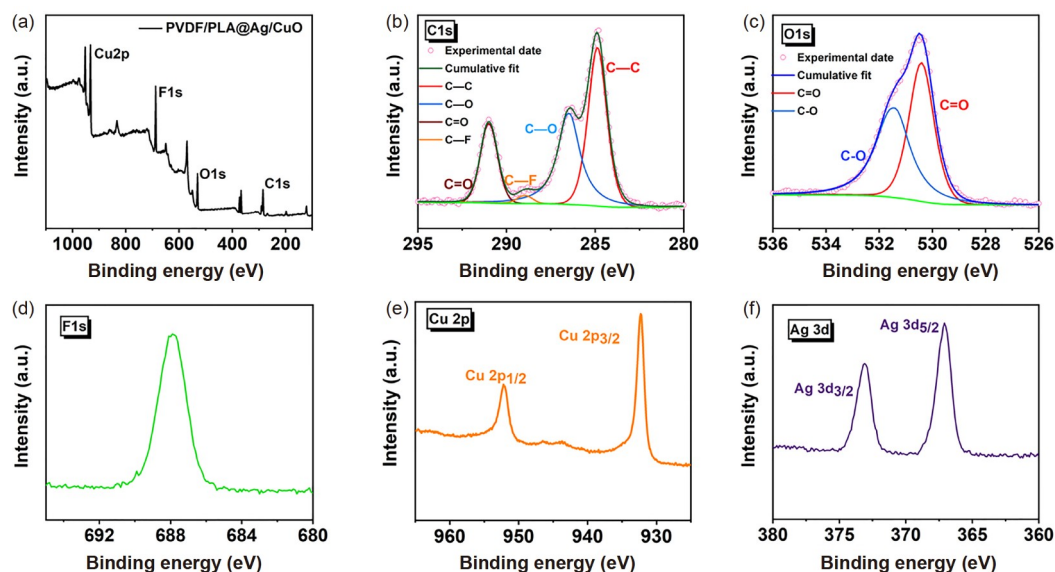

Figure 3 (Color online) X-ray photoelectron spectra of the PVDF/PLA membrane with metal nanoparticles. (a) All elemental peaks, (b) C 1s, (c) O 1s, (d) F 1s, (e) Cu 2p, (f) Ag 3d.
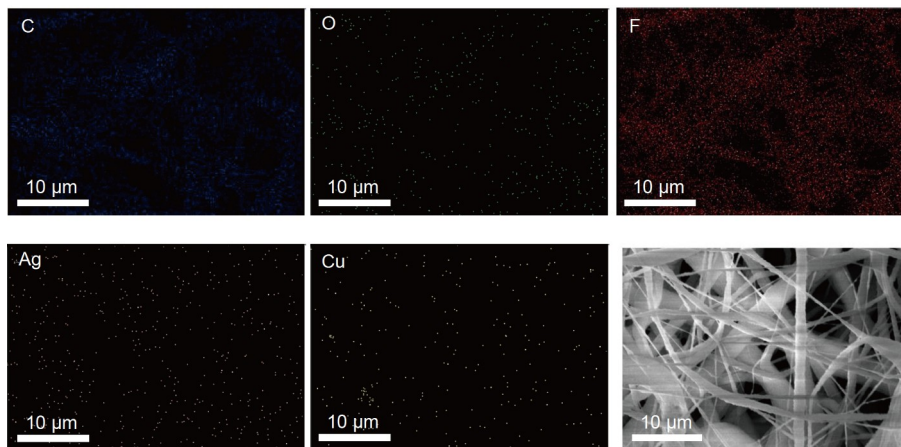
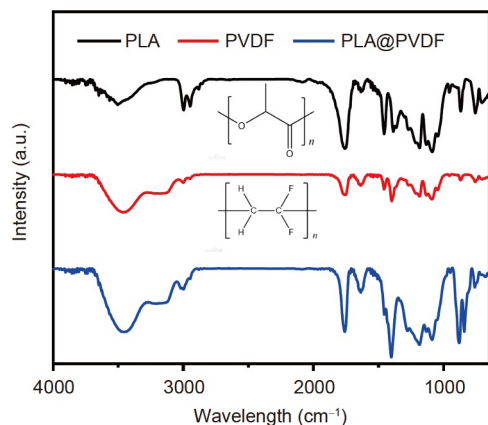**Figure 4**　Energy-dispersive spectra showing element mapping images of product membranes.

Figure 5　(Color online) Fourier transform infrared spectra of electrospun fiber membranes.

composed of three different surfactants (SDS, CTAB, Span 80) were tested at 0.1 MPa pressure. Figure 8 shows a comparison of droplets before and after emulsion separation under optical microscopy and macroscopic views. The separation efficiencies were all above 90% and the circulation volumes were above 5000 L m^{-2} h^{-1}. However, the circulation volume inevitably tended to decrease as cyclic testing proceeded, which was caused by oil contamination due to the blockage of pore channels (Figure 7(c)–(d)). Particle size distributions of the emulsion before and after separation are shown in Figure 9. The particle sizes of the emulsion were approximately 1000 nm before separation and 100 nm after separation, which is consistent with the pore size measured by BET.

3.4　Antibacterial activity

In addition to organic matter and heavy metal ions, biological contamination cannot be neglected in wastewater treatment. Therefore, this experiment investigated the antibacterial
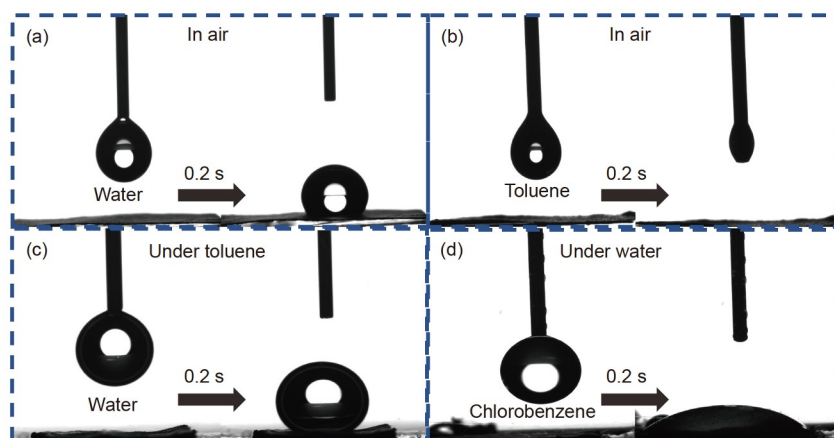
results, shown in Figure S4, indicated that the membrane surface wettability was also applicable to other organic solvents. Therefore, an emulsion separation test was conducted. The separation process is shown in Figure 7(b). Emulsions

Figure 6　Wetting performance of membrane surface. Contact angles of (a) water in air, (b) toluene in air, (c) water under toluene, (d) chlorobenzene under water.
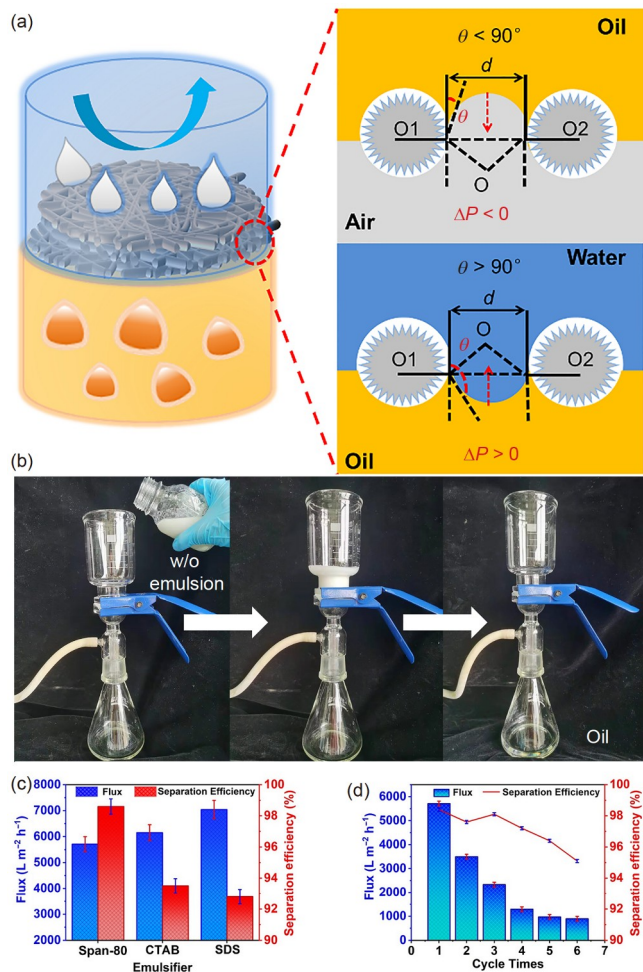
Figure 7 (Color online) (a) Model of water-in-oil emulsion separation; (b) process of emulsion separation; (c) flux and separation efficiency of three oil-in-water emulsions; (d) cycling tests of toluene-in-water emulsions.

Figure 8 (Color online) Optical micrographs and macroscopic images of emulsions before and after separation. Water in toluene with (a) Span-80, (b) CTAB, (c) SDS.

The inhibition circle radii for the three microorganisms were 0.65, 0.60, and 0.66 cm, respectively. The PVDF/PLA@Ag/CuO membrane showed a distinct inhibition zone. As the metal nanoparticle loading increased, the inhibition zone became larger (Figure S5), while the original membranes showed almost no inhibition properties. To further investigate the antibacterial performance of the composite membrane, we simulated domestic wastewater with solutions containing *E. coli* and *S. aureus*. Figure 10(c) shows the growth of the bacteria in wastewater samples before and after filtration for 12 h. By counting colonies, it was observed that the filtration efficiency of the membrane for bacteria was close to 99%, which indicates that the product membrane would offer high purification in practical application. In addition, the membrane was enriched with large numbers of microorganisms after filtration, which was collected and incubated in a 37°C thermostat for 6 h. Bacterial activity on the membrane surface was studied by bacterial staining, where green and red represent active and dead bacteria, respectively. The membrane surface was slightly rinsed with PBS solution and observed by fluorescence microscopy, as shown in Figure 10(d). Originally active *E. coli* and *S. aureus* lost most activity after 6 h of incubation on the product

performance of the membrane. Gram-positive (*Bacillus Subtilis*) and gram-negative (*E. coli*, *P. putida*) bacteria were selected as model microorganisms for qualitative analysis by inhibition circle size. As shown in Figure 10(a), antimicrobial performances of the original composite membranes and with different metal particle loadings were examined. Radii of the inhibition circles after cultivation of the bacteria on agar plates for 12 h are shown in Figure 10(b).
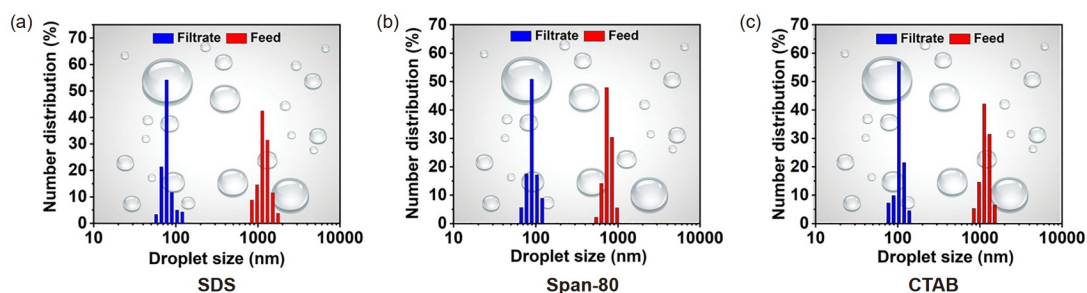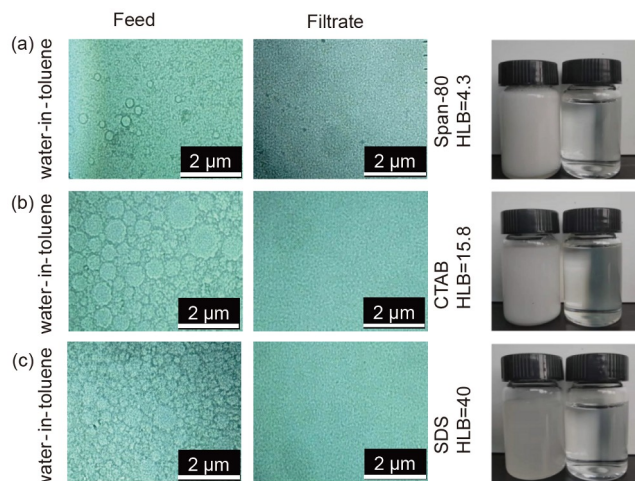

Figure 9 (Color online) Distributions of particle sizes before and after separation of (a) Span-80, (b) CTAB, and (c) SDS emulsions.

membrane. This indicates that the membrane also had the considerable bactericidal ability. This result suggests that the product membranes had some resistance to microorganisms.

The possible antibacterial mechanism is explained in Figure 11 [44–46]. Bacteria with negatively charged surfaces are able to adsorb metal particles by electrostatic forces. The metal particles then bind specifically to the thiol group (–SH) in the protease within the cell and thus pierce the cell wall. In addition, silver ions that enter the interior bind to deoxyribonucleic acid, which can interfere with the metabolism of various enzymes. The cells eventually become dysfunctional and die. Another possible scenario is that, in the presence of light or oxygen, metal particles can act as catalytic centers to generate reactive oxygen radicals. These groups can hinder the proliferation of bacteria and cause their death. When the

cells are deactivated, the silver ions are freed again, thereby achieving a sustainable antibacterial effect.

4 Conclusion

Metal nanoparticles were successfully embedded in nanofibers by thermal reduction and electrostatic spinning techniques. The obtained PVDF/PLA@Ag/CuO fiber membranes had oleophilic and hydrophobic properties and were able to separate water-in-oil emulsions with above 90% separation efficiency. In addition, the fibers contained Ag nanoparticles wrapped in PLA, which were degradable and exhibited excellent antibacterial properties. A variety of organic reagents and microbial tests showed that the product membrane gave
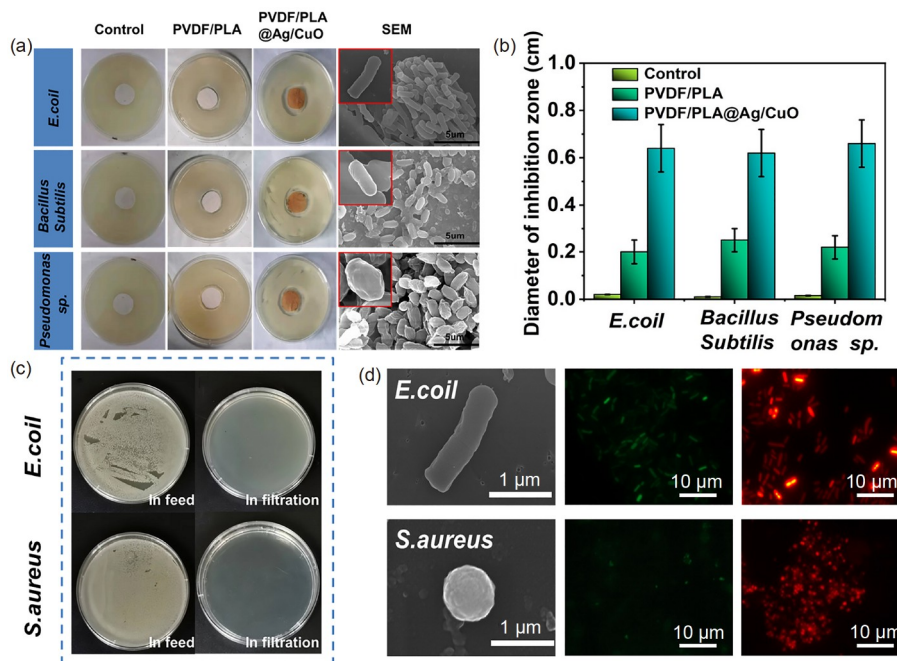

Figure 10 (Color online) (a) Digital images of inhibition circles for three bacteria; (b) diameters of inhibition zone of the membrane after 12 h; (c) growth of bacteria in wastewater samples before and after filtration for 12 h; (d) live and dead bacteria after 6 h of growth on the membrane surface under fluorescence microscopy.
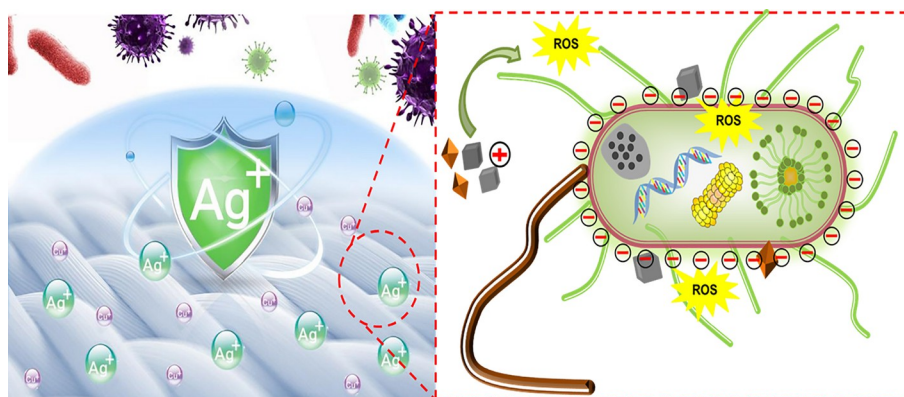

Figure 11 (Color online) Schematic explanation of antibacterial mechanism.

universal behavior. These results provide a concept for the purification of oil-containing wastewater and surface antibacterial activity.

1 Bakke T, Klungsøyr J, Sanni S. Environmental impacts of produced water and drilling waste discharges from the Norwegian offshore petroleum industry. Mar Environ Res, 2013, 92: 154–169

2 Jernelöv A. How to defend against future oil spills. Nature, 2010, 466: 182–183

3 Carpenter A. Oil pollution in the North Sea: The impact of governance measures on oil pollution over several decades. Hydrobiologia, 2019, 845: 109–127

4 Monteiro C B, Oleinik P H, Leal T F, et al. Integrated environmental vulnerability to oil spills in sensitive areas. Environ Pollut, 2020, 267: 115238

5 Crini G, Lichtfouse E. Advantages and disadvantages of techniques used for wastewater treatment. Environ Chem Lett, 2019, 17: 145–155

6 Liang B, He X, Hou J, et al. Membrane separation in organic liquid: Technologies, achievements, and opportunities. Adv Mater, 2019, 31: 1806090

7 Padaki M, Surya Murali R, Abdullah M S, et al. Membrane technology enhancement in oil-water separation: A review. Desalination, 2015, 357: 197–207

8 Wei Y, Qi H, Gong X, et al. Specially wettable membranes for oil-water separation. Adv Mater Interfaces, 2018, 5: 1800576

9 Spark A J, Law D W, Ward L P, et al. Effect of *Pseudomonas fluorescens* on buried steel pipeline corrosion. Environ Sci Technol, 2017, 51: 8501–8509

10 Topić Popović N, Kazazić S P, Barišić J, et al. Aquatic bacterial contamination associated with sugarplant sewage outfalls as a microbial hazard for fish. Chemosphere, 2019, 224: 1–8

11 Sib E, Lenz-Plet F, Barabasch V, et al. Bacteria isolated from hospital, municipal and slaughterhouse wastewaters show characteristic, different resistance profiles. Sci Total Environ, 2020, 746: 140894

12 Spark A, Wang K, Cole I, et al. Microbiologically influenced corrosion: A review of the studies conducted on buried pipelines. Corrosion Rev, 2020, 38: 231–262

13 Cai Y, Shi S Q, Fang Z, et al. Design, development, and outlook of superwettability membranes in oil/water emulsions separation. Adv Mater Interfaces, 2021, 8: 2100799

14 Liu M, Wang S, Jiang L. Nature-inspired superwettability systems. Nat Rev Mater, 2017, 2: 17036

15 Tian X, Jokinen V, Li J, et al. Unusual dual superlyophobic surfaces in oil-water systems: The design principles. Adv Mater, 2016, 28: 10652–10658

16 Chen H, Huang M, Liu Y, et al. Functionalized electrospun nanofiber membranes for water treatment: A review. Sci Total Environ, 2020, 739: 139944

17 Su R, Li S, Wu W, et al. Recent progress in electrospun nanofibrous membranes for oil/water separation. Sep Purif Tech, 2021, 256: 117790

18 Sun X, Bai L, Li J, et al. Robust preparation of flexibly super-hydrophobic carbon fiber membrane by electrospinning for efficient oil-water separation in harsh environments. Carbon, 2021, 182: 11–22

19 Zhang J, Liu L, Si Y, et al. Rational design of electrospun nanofibrous materials for oil/water emulsion separation. Mater Chem Front, 2021,
5: 97–128

20 Zhao R, Tian Y, Li S, et al. An electrospun fiber based metal-organic framework composite membrane for fast, continuous, and simultaneous removal of insoluble and soluble contaminants from water. J Mater Chem A, 2019, 7: 22559–22570

21 Li H, Chen X, Lu W, et al. Application of electrospinning in antibacterial field. Nanomaterials, 2021, 11: 1822

22 Patil N A, Gore P M, Jaya Prakash N, et al. Needleless electrospun phytochemicals encapsulated nanofibre based 3-ply biodegradable mask for combating COVID-19 pandemic. Chem Eng J, 2021, 416: 129152

23 Yue Y, Gong X, Jiao W, et al. *In-situ* electrospinning of thymol-loaded polyurethane fibrous membranes for waterproof, breathable, and antibacterial wound dressing application. J Colloid Interface Sci, 2021, 592: 310–318

24 Zhang Z, Ji D, He H, et al. Electrospun ultrafine fibers for advanced face masks. Mater Sci Eng-R-Rep, 2021, 143: 100594

25 Zhu M, Hua D, Pan H, et al. Green electrospun and crosslinked poly-(vinyl alcohol)/poly(acrylic acid) composite membranes for antibacterial effective air filtration. J Colloid Interface Sci, 2018, 511: 411–423

26 Wu F, He P, Chang X, et al. Visible-light-driven and self-hydrogen-donated nanofibers enable rapid-deployable antimicrobial bioprotection. Small, 2021, 17: 2100139

27 Karagoz S, Kiremitler N B, Sarp G, et al. Antibacterial, antiviral, and self-cleaning mats with sensing capabilities based on electrospun nanofibers decorated with ZnO nanorods and Ag nanoparticles for protective clothing applications. ACS Appl Mater Interfaces, 2021, 13: 5678–5690

28 Liu Y, Wang D, Sun Z, et al. Preparation and characterization of gelatin/chitosan/3-phenylacetic acid food-packaging nanofiber antibacterial films by electrospinning. Int J Biol Macromol, 2021, 169: 161–170

29 Pakravan M, Heuzey M C, Ajji A. Core-shell structured PEO-chitosan nanofibers by coaxial electrospinning. Biomacromolecules, 2012, 13: 412–421

30 Cao W, Ma W, Lu T, et al. Multifunctional nanofibrous membranes with sunlight-driven self-cleaning performance for complex oily wastewater remediation. J Colloid Interface Sci, 2022, 608: 164–174

31 Liu F, Liu Y, Sun Z, et al. Preparation and antibacterial properties of ε-polylysine-containing gelatin/chitosan nanofiber films. Int J Biol Macromol, 2020, 164: 3376–3387

32 Xin Q, Shah H, Nawaz A, et al. Antibacterial carbon-based nanomaterials. Adv Mater, 2019, 31: 1804838

33 Ye Z, Li S, Zhao S, et al. Textile coatings configured by double-nanoparticles to optimally couple superhydrophobic and antibacterial properties. Chem Eng J, 2021, 420: 127680

34 Zhang M, Wang G, Wang D, et al. Ag@MOF-loaded chitosan nanoparticle and polyvinyl alcohol/sodium alginate/chitosan bilayer dressing for wound healing applications. Int J Biol Macromol, 2021, 175: 481–494

35 Chen Z, Balankura T, Fichthorn K A, et al. Revisiting the polyol synthesis of silver nanostructures: Role of chloride in nanocube formation. ACS Nano, 2019, 13: 1849–1860

36 Chen Z, Chang J W, Balasanthiran C, et al. Anisotropic growth of silver nanoparticles is kinetically controlled by polyvinylpyrrolidone binding. J Am Chem Soc, 2019, 141: 4328–4337

37 Im S H, Lee Y T, Wiley B, et al. Large-scale synthesis of silver nanocubes: The role of HCl in promoting cube perfection and monodispersity. Angew Chem Int Ed, 2005, 44: 2154–2157

38 Ruditskiy A, Xia Y. Toward the synthesis of sub-15 nm Ag nanocubes with sharp corners and edges: The roles of heterogeneous nucleation and surface capping. J Am Chem Soc, 2016, 138: 3161–3167

39 Wang Y, Wan D, Xie S, et al. Synthesis of silver octahedra with controlled sizes and optical properties via seed-mediated growth. ACS Nano, 2013, 7: 4586–4594

40 Xia X, Zeng J, Oetjen L K, et al. Quantitative analysis of the role

played by poly(vinylpyrrolidone) in seed-mediated growth of Ag nanocrystals. J Am Chem Soc, 2012, 134: 1793–1801

41   Zhou S, Li J, Gilroy K D, et al. Facile synthesis of silver nanocubes with sharp corners and edges in an aqueous solution. ACS Nano, 2016, 10: 9861–9870

42   Zhang D F, Zhang H, Guo L, et al. Delicate control of crystallographic facet-oriented Cu_2O nanocrystals and the correlated adsorption ability. J Mater Chem, 2009, 19: 5220–5225

43   Wang Y, Liu Z, Wei X, et al. An integrated strategy for achieving oil-in-water separation, removal, and anti-oil/dye/bacteria-fouling. Chem Eng J, 2021, 413: 127493

44   Park B C, Byun S W, Ju Y, et al. Zinc oxide nano-spicules on poly-lactic acid for super-hydrophilic and bactericidal surfaces. Adv Funct Mater, 2021, 31: 2100844

45   Trandafilović L V, Whiffen R K, Dimitrijević-Branković S, et al. ZnO/Ag hybrid nanocubes in alginate biopolymer: Synthesis and properties. Chem Eng J, 2014, 253: 341–349

46   Yu W, Li X, He J, et al. Graphene oxide-silver nanocomposites embedded nanofiber core-spun yarns for durable antibacterial textiles. J Colloid Interface Sci, 2021, 584: 164–173